High-Quality Factor Superconducting Flexible Resonators Embedded in Thin-Film Polyimide HD-4110

Simin Zou, *Student Member, IEEE*, Yang Cao, Vaibhav Gupta, *Student Member, IEEE*, Bhargav Yelamanchili, *Student Member, IEEE*, John A. Sellers, Charles D. Ellis, David B. Tuckerman, *Fellow, IEEE*, and Michael C. Hamilton, *Senior Member, IEEE*

***Abstract*—We present the design, fabrication procedure, and measurement results of Nb superconducting microstrip transmission line resonators fabricated using thin-film polyimide HD-4110, including both nonembedded and embedded versions. These resonators were used to characterize the microwave dielectric loss tangent of 20 μm thick polyimide HD-4110 at deep cryogenic temperatures. We observed high-quality factors (Q) up to 21 040 at 1.2 K in the frequency range of 2–21 GHz for nonembedded resonators, indicating that the dielectric loss tangent can be less than 5×10^{-5}. Embedded resonators with an additional 20 μm thick encapsulation layer also exhibited Q values as high as $\sim$19 200. Dielectric and conductor (quasiparticle) loss have been compared between the two types of resonators. This study provides information applicable to the design of future high-density, flexible, multilayer superconducting cables, which are of great interest for potential applications in cryogenic electronics systems, including quantum computers.**

***Index Terms*—Flexible, loss tangent, microstrip, niobium, polyimide, resonators, superconducting.**

I. Introduction

ONE of the major limitations in building densely integrated, cryogenic electronics systems is the electrical interconnect technology, especially for high-speed and microwave systems [1]–[3]. Polyimide has been widely used for electronics packaging [4]–[6] and flexible electronics [7]–[11] applications due to its excellent mechanical and electrical properties. Its low thermal conductivity is beneficial for constructing flexible superconducting transmission lines that connect between different temperature stages in a dilution refrigerator, such as those used in quantum computing systems. In [3], we reported the low-temperature microwave dielectric properties of two common types of polyimide, PI-2611 [12] and HD-4100 [13], using nonembedded flexible microstrip transmission line resonators. Embedded microstrip is of considerably more practical interest than nonembedded microstrip, as the former is more mechanically robust and provides a stepping stone in fabricating more complex controlled-impedance interconnect structures such as stripline. In previous work [14], [15], we have addressed the need for embedded structures and reported using nonphotosensitive polyimide PI-2611 to build embedded Nb flexible cables. Although we were able to make functional embedded resonators and low-loss transmission lines using polyimide PI-2611, they suffered from two major drawbacks: the microwave performance of these embedded resonators degraded noticeably after addition of a relatively thin embedding layer (4 or 8 μm), and the nonphotosensitive property of PI-2611 is an impediment in building more sophisticated structures (i.e., incorporating vias). The use of HD-4110 polyimide [13] addresses these issues. HD-4110 is a photosensitive dielectric and permits relatively thick (20 μm) layers to be deposited with one spin, which can simplify the fabrication procedure for constructing multilayer interconnect structures, such as stripline or multichip modules.

In this paper, we report on the design, fabrication procedure, and microwave performance of embedded flexible Nb superconducting microstrip transmission line resonators fabricated using HD-4110 polyimide, and compare the results with corresponding nonembedded structures. Excellent microwave performance is achieved for both of these two types of structures. Dielectric loss tangent and quasiparticle loss for the resonator structures are also characterized from 2 to 21 GHz at several cryogenic temperatures between 1.2 and 4.2 K.

II. Design and Fabrication Procedure

Half-wavelength, capacitively coupled microstrip transmission line resonators were designed and fabricated. The layout of nonembedded and embedded versions of resonators was identical and a top view of the design is shown in Fig. 1(a). A three-dimensional perspective image of an embedded resonator is shown in Fig. 1(b). All dimensions for the two types of resonators are the same except the embedded resonator has a 20 μm encapsulation layer of HD-4110. Key dimensions of the resonator designs are listed in Table I. The resonator

Manuscript received May 12, 2017; revised July 6, 2017; accepted July 7, 2017. Date of publication August 18, 2017; date of current version August 30, 2017. This work was supported by the Microsoft Research. This paper was recommended by Associate Editor S. Anlage. *(Corresponding author: Simin Zou.)*

S. Zou, Y. Cao, V. Gupta, B. Yelamanchili, J. A. Sellers, C. D. Ellis, and M. C. Hamilton are with the Department of Electrical and Computer Engineering, Auburn University, AL 36849 USA (e-mail: szz0013@tigermail.auburn.edu; mchamilton@auburn.edu).

D. B. Tuckerman is with Microsoft Research, Redmond, WA 98052 USA.

Color versions of one or more of the figures in this paper are available online at http://ieeexplore.ieee.org.

Digital Object Identifier 10.1109/TASC.2017.2732281

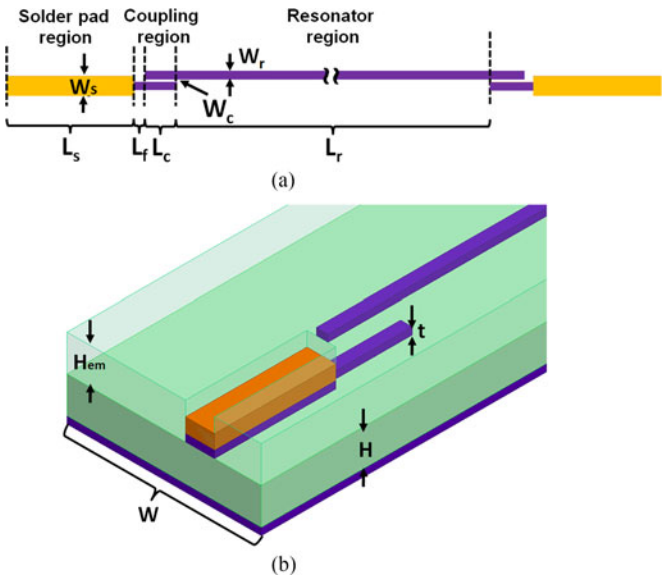

Fig. 1. (a) Top view of the half-wavelength, capacitively-coupled microstrip transmission line resonators on thin-film HD-4110. (b) Three-dimensional view of one end of embedded resonator.

TABLE I
KEY DIMENSIONS OF THE RESONATOR DESIGNS

Symbol	Value	Description
W	6 mm	Width of dielectric
H	20 μm	Height of dielectric
t	0.25 μm	Thickness of Nb layer
$H_{\rm em}$	0, 20 μm	Thickness of HD-4110 encapsulation layer
$W_{\rm s}$	120 μm	Width of solder pad
Ls	1200 μm	Length of solder pad
$L_{\rm f}$	100 μm	Length of feed line
$L_{\rm c}$	300 μm	Length of coupling gap
$W_{\rm c}$	20 μm	Width of coupling gap
$W_{\rm r}$	47.4 μm	Width of resonator
$L_{\rm r}$	46.1 mm	Length of resonator

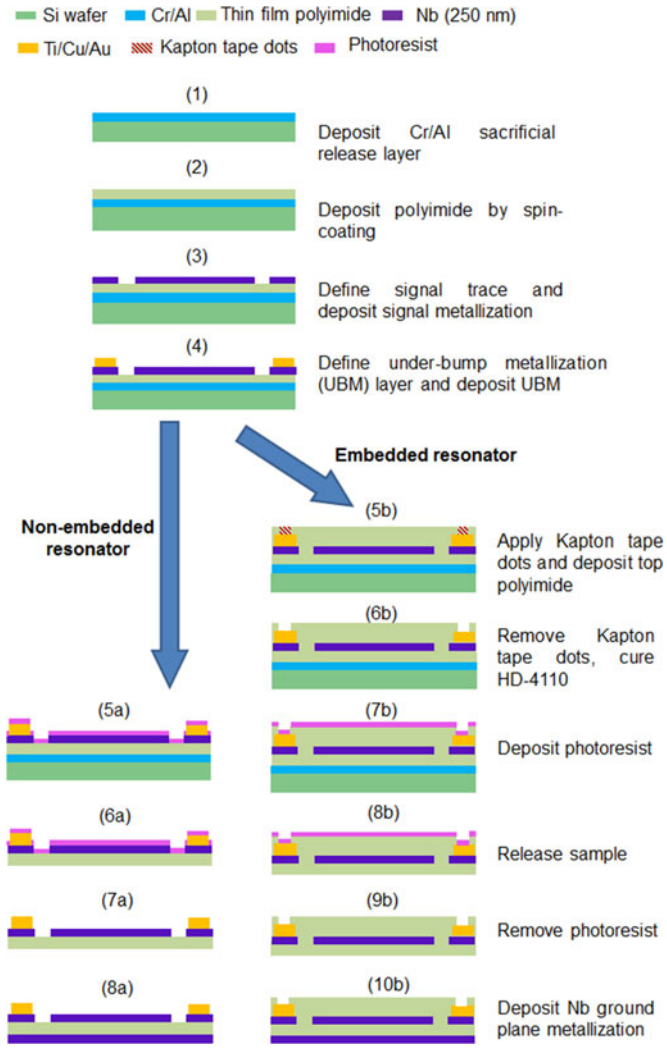

Fig. 2. Schematic of fabrication procedures for nonembedded and embedded Nb microstrip transmission line resonators.

length was chosen to yield a fundamental resonant frequency (f_0) of ~2 GHz. The width of the signal line was designed to provide a characteristic impedance of 50 Ω, in order to be representative of corresponding 50 Ω transmission lines.

Fig. 2 schematically illustrates the fabrication procedures for superconducting Nb microstrip transmission line resonators fabricated using HD-4110 polyimide, including nonembedded [see Fig. 2(1)–(8a)] and embedded [see Fig. 2(1)–(10b)] configurations. Starting with two oxidized Si handle wafers, 25 nm thick Cr and 200-nm thick Al were deposited on these wafers as a sacrificial release layer [16]. Polyimide HD-4110 was spun onto both wafers to achieve a ~20 μm thick film, followed by curing at 375 °C in an N_2 environment. Resonator signal lines of ~250 nm thick Nb connected to Ti(50 nm)/Cu(500 nm)/Au(10 nm) underbump metal (UBM) pad stacks were formed using conventional photolithography and film lift-off techniques. The Nb film was rf sputter deposited with a power of ~8 W/cm^2 and Ar pressure of 4 mTorr [17]. The UBM pads were deposited by electron-beam thermal evaporation after a 2 min *in situ* ion beam milling surface clean. For the embedded microstrip transmission line resonators, small Kapton tape "dots" were then used to cover the UBM pad area to be used for electrical connection, followed by spin-on deposition of a top HD-4110 encapsulation layer. The embedding layer was cured at lower temperature (225 °C) to protect the superconductivity of the embedded Nb, and was ~20 μm thick postcure. Subsequently, both nonembedded and embedded samples were protected with a layer of photoresist during a film release process (soaking in a sodium chloride solution with 0.5 V applied to the Cr/Al release layer). After release and stripping of the photoresist, the samples were then inverted and mounted onto Si handle wafers, followed by a ground plane deposition of ~250 nm thick Nb. Resonators were then assembled with end-launch SMA connectors from Southwest Microwave, Inc. [18] in order to make reliable microwave connections at low temperature. Fig. 3 shows a photograph of an assembled nonembedded Nb resonator. We note that, due to the test fixture configuration, the flexible resonator is in a slightly bent configuration.

III. RESULTS AND DISCUSSION

S_{21} and S_{12} response of nonembedded resonators were measured at different temperatures (1.2, 2.0, 3.0, and 4.2 K) up to 21 GHz in a pulse-tube-based cryostat using an Agilent

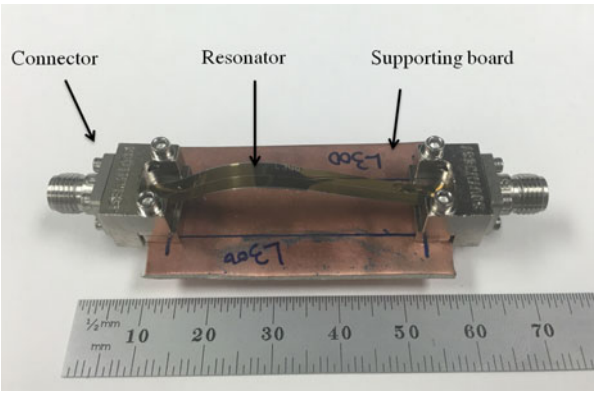

Fig. 3. Flexible nonembedded Nb microstrip transmission line resonator assembly with Southwest microwave SMA end-launch connectors.

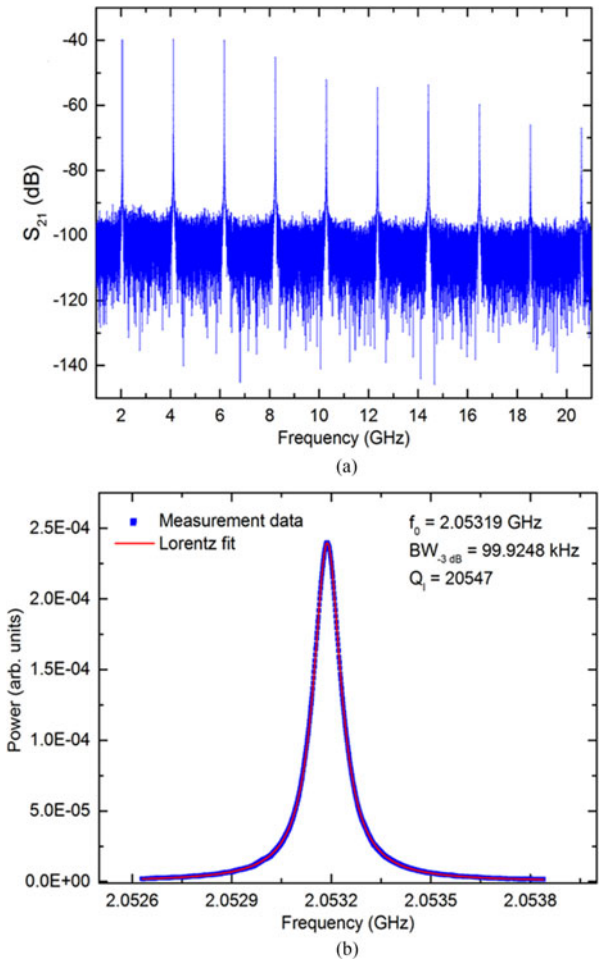

Fig. 4. S_{21} measurement results of a nonembedded Nb/HD-4110 flexible microstrip resonator measured at 1.2 K. (a) Broadband view of S_{21} response versus frequency from first to tenth mode. (b) Fundamental resonance (first mode) measurement result and corresponding Lorentz fit. The best-fit center frequency, 3 dB bandwidth and loaded Q information are provided.

(Keysight) N5227A performance network analyzer. Before resonators were loaded into the cryostat, a 2 h dehydration bake at 90 °C in a vacuum was performed to minimize the humidity effects. Fig. 4(a) shows S_{21} measurement results of a nonembedded Nb resonator at 1.2 K. In order to precisely determine loaded quality factor (Q_l) information, a sufficient number of

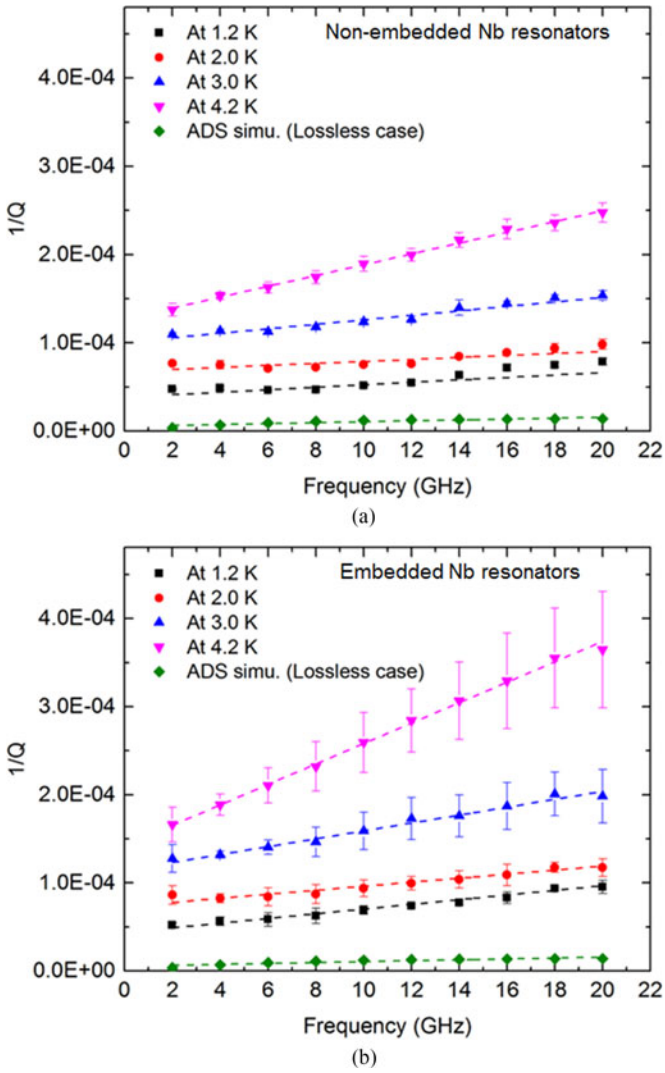

Fig. 5. $1/Q_l$ for multiple resonant frequencies of (a) nonembedded and (b) embedded Nb resonators at different temperatures, along with corresponding ADS simulation results with no conductor or dielectric loss. Note the increase of slopes and variance in the embedded resonators, which indicate higher quasiparticle losses in the Nb.

data points were taken for each resonance peak. Fig. 4(b) shows the fundamental resonance, along with a Lorentz fit, of a nonembedded Nb resonator with a Q_l value of 20 547 at 1.2 K and at an incident power of -30 dBm.

Fig. 5(a) shows a plot of $1/Q_l$ versus frequency measured at multiple temperatures. Sample-to-sample variation and temperature drift in the pulse-tube cryostat have been considered and each marker in the figure is the average value from ten measurements of three resonators with a 3σ error bar. Keysight ADS simulation results with zero conductor loss and $\tan\delta = 0$ (i.e., exhibiting only coupling loss) are also shown in Fig. 5(a) as a reference. As can be seen from the figure, $1/Q_l$ versus resonant frequency plots all appear as essentially straight lines at each temperature, as shown by the dashed linear fit lines.

The following analysis is based on superconducting transmission line resonator theory along with an assumption that the dielectric loss tangent is relatively constant over the measured range of frequencies. From this, we find that the slopes

TABLE II
SIMULATED Q_{coupling}, MEASURED Q_{l}, AND EXTRACTED UPPER BOUND ON $\tan\delta$ AT RESONANT FREQUENCIES AT 1.2 AND 2.0 K FOR NONEMBEDDED AND EMBEDDED NB TRANSMISSION LINE RESONATORS

Q_{coupling}	Nonembedded			Embedded		
	$\sim f_0$ (GHz)	Q_{l} ($\tan\delta$) @ 1.2 K	Q_{l} ($\tan\delta$) @ 2.0 K	$\sim f_0$ (GHz)	Q_{l} ($\tan\delta$) @ 1.2 K	Q_{l} ($\tan\delta$) @ 2.0 K
267 846	2.0	21 040 (4.97E−05)	13 010 (8.29E−05)	1.9	19 209 (5.15E−05)	11 588 (8.79E−05)
143 400	4.0	20 427 (4.76E−05)	13 372 (7.69E−05)	3.8	17 723 (5.27E−05)	12 133 (8.03E−05)
105 959	6.0	21 575 (4.19E−05)	14 052 (7.00E−05)	5.7	17 066 (5.22E−05)	11 855 (7.98E−05)
89 884	8.0	21 351 (4.05E−05)	13 821 (6.94E−05)	7.6	15 974 (5.47E−05)	11 454 (8.11E−05)
81 977	10.0	19 436 (4.45E−05)	13 265 (7.17E−05)	9.5	14 507 (6.05E−05)	10 646 (8.70E−05)
77 781	12.0	18 271 (4.75E−05)	13 136 (7.17E−05)	11.4	13 522 (6.52E−05)	10 056 (9.22E−05)
75 337	14.0	15 759 (5.69E−05)	11 810 (8.10E−05)	13.3	12 883 (6.84E−05)	9626 (9.65E−05)
73 659	16.0	13 908 (6.61E−05)	11 239 (8.55E−05)	15.2	12 021 (7.43E−05)	9180 (1.02E−04)
72 186	18.0	13 339 (6.93E−05)	10 663 (9.06E−05)	17.1	10 697 (8.48E−05)	8510 (1.10E−04)
70 578	20.0	12 668 (7.34E−05)	10 208 (9.50E−05)	19.0	10 497 (8.63E−05)	8521 (1.10E−04)

and zero-frequency intercepts of the 1/Q plots correspond to the superconductor quasiparticle loss (i.e., from BCS theory) and dielectric loss, respectively. Details in support of these statements can be found in [3] and [19]. Slopes and the zero-frequency intercepts are observed to decrease as the temperature decreases from 4.2 to 2.0 K. Fitting lines of the 1.2 and 2.0 K data are nearly parallel with the simulation data ($\tan\delta = 0$). This indicates that Nb quasiparticle loss is negligible at these temperatures and the loss in the resonator is dominated by HD-4110 dielectric loss. Low quasiparticle loss is also in agreement with high intrinsic Nb Q_0 reported in [20]. The unloaded quality (Q_0) of the resonators includes the impact of conductor, dielectric, and radiation loss [21], as shown in (1)

$$\frac{1}{Q_0} = \frac{1}{Q_c} + \frac{1}{Q_d} + \frac{1}{Q_r} \tag{1}$$

where Q_c, Q_d, and Q_{r} are Q associated with conductor loss, dielectric loss, and radiation loss, respectively. Q_0 also can be expressed as the following equation [22]:

$$\frac{1}{Q_0} = \frac{1}{Q_l} - \frac{1}{Q_e} \tag{2}$$

where Q_{e} is external Q, which is dominated by coupling Q (Q_{coupling}). Therefore, Q_{l} can be expressed as the following equation:

$$\frac{1}{Q_l} = \frac{1}{Q_c} + \frac{1}{Q_d} + \frac{1}{Q_r} + \frac{1}{Q_{\mathrm{coupling}}}. \tag{3}$$

Radiation loss was determined to be negligible for these resonators, owing to their very small cross sections. Conductor loss is also negligible below ∼2.0 K, which is well below the critical transition temperature. Therefore, Q_0 is dominated by Q_{d}, which can be found from the measured Q_{l} and simulated Q_{coupling}. From Q_{d}, the dielectric loss tangent ($\tan\delta$) can be extracted using the following equation [21]:

$$Q_d = \frac{1}{\tan\delta}\left(1 + \frac{1-q}{q\epsilon_r}\right) \tag{4}$$

where ϵ_r is the relative permittivity for the polyimide and q is a microstrip filling factor. An ϵ_r value of 3.2 was found using an iterative process to match ADS simulation results to measurement results for a Cu resonator. More details can be found in [23]. The filling factor q of these nonembedded and embedded microstrip transmission lines are 0.703 and 0.828, respectively.

Detailed Q_{coupling}, Q_{l} and $\tan\delta$ values at 1.2 and 2.0 K and at each resonant frequency are listed in the second and third columns in Table II. We note that, since we cannot completely rule out other parasitic losses not related to the dielectric, the actual loss tangent could be less than the extracted values. These results provide important information for cryogenic high-frequency structure simulation and design with HD-4110. Furthermore, they indicate that HD-4110 is a promising dielectric material for flexible cryogenic electronics, packaging, and interconnect structures.

In order to evaluate the performance of embedded resonators and to determine the influence of the lower temperature cured encapsulation layer and additional fabrication processing, three embedded Nb resonators were measured at the same temperatures and in the same frequency range, as shown in Fig. 5(b). We can see larger variance in this plot compared to nonembedded resonators, which is likely due to the additional embedding fabrication process. An increase in slope of the 1/Q_{l} versus frequency lines is also evident, especially at higher temperatures. Through analysis of the results shown in Fig. 5, slope and intercept values of both types of Nb resonators were obtained (see Fig. 6). As temperature increases from 1.2 to 4.2 K for each material stack-up, loss due to the HD-4110 dielectric increases gradually, as is evident from the increased intercept values. Growth of conductor (quasiparticle) loss starts from 2.0 K for these resonators, as evident from the increased slopes. Furthermore, at each temperature, with the use of a 225 °C cured encapsulation layer, the combined dielectric loss increases slightly. The authors believe it is possible that solvent and moisture may still exist in lower temperature cured HD-4110, which may be the source of the additional dielectric loss and increased variation for the embedded samples. Also, it can be seen that the quasiparticle loss increases for the embedded structures, and this may be due to the availability of degrading substances (i.e., acids and/or H_2O) in the embedding layer during the curing process that could lead to the degradation of the superconducting properties of the Nb, even with a lower temperature curing process. Measured Q_{l} and computed $\tan\delta$ of embedded resonators

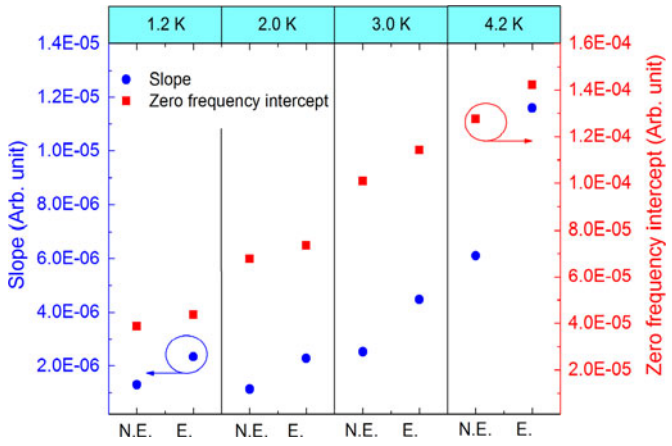

Fig. 6. Comparison of slope and zero-frequency intercept values of linear fitting lines of $1/Q_l$ versus frequency plot of nonembedded and embedded Nb resonators at different temperatures. N.E. is for nonembedded and E. is for embedded.

corrected with Q_{coupling} and filling factor q at 1.2 and 2.0 K are shown in Table II. Even with the slight degradation due to the low-temperature cure of HD-4110 on top of Nb, the performance of embedded transmission lines fabricated with this process would be quite suitable for propagating microwave signals in cryogenic and superconducting electronics systems over meter-scale distances.

IV. Conclusion

In this paper, upper bounds on the microwave loss tangent of polyimide HD-4110 were reported at deep cryogenic temperature for a wide frequency range, showing values as low as 5×10^{-5}. By using a reduced cure temperature for an HD-4110 polyimide embedding layer, we achieved microwave performance that is very comparable to that of nonembedded flexible superconducting microstrip. The data presented in this paper not only provide design guidance for constructing ultralow-loss flexible thin-film superconducting interconnects using embedded microstrip, but also show the feasibility of building cables with more complex structures, such as stripline.

Acknowledgment

The authors would like to acknowledge the technical guidance from Microsoft Research for this work.

References

[1] P. McGarey, H. Mani, C. Wheeler, and C. Groppi, "A 16-channel flex circuit for cryogenic microwave signal transmission," in *Proc. SPIE*, vol. 9153, 2014, Art. no. 91532F. doi: 10.1117/12.2055472.

[2] T. S. Tighe, G. Akerling, and A. D. Smith, "Cryogenic packaging for multi-GHz electronics," *IEEE Trans. Appl. Supercond.*, vol. 9, no. 3, pp. 3173–3176, Jun. 1999. doi: 10.1109/77.783703.

[3] D. B. Tuckerman *et al.*, "Flexible superconducting Nb transmission lines on thin film polyimide for quantum computing applications," *Supercond. Sci. Technol.*, vol. 29, no. 8, 2016, Art. no. 084007. doi:10.1088/0953-2048/29/8/084007.

[4] S. Priyabadini, T. Sterken, M. Cauwe, L. Van Hoorebeke, and J. Van-fleteren, "High-yield fabrication process for 3d-stacked ultrathin chippackages using photo-definable polyimide and symmetry in package," *IEEE Trans. Compon. Packag. Manuf. Technol.*, vol. 4, no. 1, pp. 158–167, Jan. 2014. doi: 10.1109/TCPMT.2013.2284068.

[5] W. Christiaens, T. Loeher, B. Pahl, M. Feil, B. Vandevelde, and J. Vanfleteren, "Embedding and assembly of ultrathin chips in multilayer flex boards," *Circuit World*, vol. 34, no. 3, pp. 3–8, 2008. doi: 10.1108/03056120810896209.

[6] L. Wang, T. Sterken, M. Cauwe, D. Cuypers, and J. Vanfleteren, "Fabrication and characterization of flexible ultrathin chip package using photosensitive polyimide," *IEEE Trans. Compon. Packag. Manuf. Technol.*, vol. 2, no. 7, pp. 1099–1106, Jul. 2012. doi: 10.1109/TCPMT.2012.2188402.

[7] S. Zou *et al.*, "Influence of fatigue and bending strain on critical currents of niobium superconducting flexible cables containing Ti and Cu interfacial layers," *IEEE Trans. Appl. Supercond.*, vol. 27, no. 4, Jun. 2017, Art. no. 6000605. doi: 10.1109/TASC.2016.2641239.

[8] H. Cao, A.-L. Li, C. Nguyen, Y.-B. Peng, and J.-C. Chiao, "An integrated flexible implantable micro-probe for sensing," *IEEE Sensors J.*, vol. 12, no. 5, pp. 1618–1624, May 2012. doi: 10.1109/JSEN.2011.2173674.

[9] S. Zou, P. Xu, and M. C. Hamilton, "Resistive switching characteristics in printed Cu/CuO/(AgO)/Ag memristors," *Electron. Lett.*, vol. 49, no. 13, pp. 829–830, 2013. doi: 10.1049/el.2013.1302.

[10] V. Misra *et al.*, "Flexible technologies for self-powered wearable health and environmental sensing neurotransmitters," *Proc. IEEE*, vol. 103, no. 4, pp. 665–681, Apr. 2015. doi: 10.1109/JPROC.2015.2412493.

[11] S. Zou and M. C. Hamilton, "Flexible non-volatile Cu/Cu_xO/Ag ReRAM memory devices fabricated using ink-jet printing technology," in *Proc. IEEE 64th Electron. Components Technol. Conf.*, 2014, pp. 441–446. doi: 10.1109/ECTC.2014.6897321.

[12] HD MicroSystems, "PI-2600 Series—Low stress applications product bulletin," 2009. [Online]. Available: http://www.dupont.com/content/dam/dupont/products-and-services/electronic-and-electrical-materials/semiconductor-fabrication-and-packaging-materials/documents/PI-2600_ProcessGuide.pdf

[13] HD MicroSystems, "HD-4100 Series product bulletin," 2014. [Online]. Available: http://www.hdmicrosystems.com/HDMicroSystems/en_US/products/photodefineable/HD-4100_negative_solvent.html

[14] V. Gupta *et al.*, "Preserving niobium superconductivity in thin-film superconducting flexible cables," in *Proc. IMAPS 12th Int. Conf. Exhib. Device Packag.*, 2016, pp. 002075–002094. doi: 10.4071/2016DPC-THA32.

[15] S. Zou *et al.*, "Embedded niobium using PI-2611 for superconducting flexible cables," *MRS Adv.*, vol. 2, pp. 2219–2204, 2017. doi: 10.1557/adv.2017.131.

[16] S. Metz, A. Bertsch, and P. Renau, "Partial release and detachment of microfabricated metal and polymer structures by anodic metal dissolution," *J. Microelectromech. Syst.*, vol. 14, no. 2, pp. 383–391, 2005. doi: 10.1109/JMEMS.2004.839328.

[17] V. Gupta *et al.*, "Minimizing film stress and degradation in thin-film Nb superconducting cables," in *Proc. IMAPS 13th Int. Conf. Exhib. Device Packag.*, 2017.

[18] Southwest Microwave, Inc., *End Launch Connectors*. [Online]. Available: http://mpd.southwestmicrowave.com/products/family.php?family=71

[19] D. M. Pozar, *Microwave Engineering*, 4th ed. Hoboken, NJ, USA: Wiley, 2012, p. 280.

[20] J. P. Turneaure, "Measurements on superconducting Nb prototype structures at 1300 MHz," *IEEE Trans. Nucl. Sci.*, vol. 18, no. 3, pp. 166–167, Jun. 1971. doi: 10.1109/TNS.1971.4325997.

[21] E. Belohoubek and E. Denlinge, "Loss considerations for microstrip resonators (short papers)," *IEEE Trans. Microw. Theory Techn.*, vol. MTT-23, no. 6, pp. 522–526, Jun. 1975. doi: 10.1109/TMTT.1975.1128615.

[22] D. M. Pozar, *Microwave Engineering*, 4th ed. Hoboken, NJ, USA: Wiley, 2012, p. 278.

[23] R. Bai, "Superconducting resonators on thin film flexible substrates," Ph.D. dissertation, Auburn Univ., Auburn, AL, USA, 2016. [Online]. Available: http://hdl.handle.net/10415/5470

Authors' biographies not available at the time of publication.